σ^- emission spectra from an array of QDs with $R = 80$ nm at $B = 8$ T. At small P the both σ^+- and σ^- spectra display the single exciton line (X^+ or X^-) in accordance with the allowed transition scheme in Fig. 8. The splitting of the X^+ and X^- lines, Δ_s, connected to the Zeeman splitting of electron and hole states, reaches 0.7 meV at $B = 8$ T. A larger intensity of the σ^+ component reflects a higher filling of the ground exciton state. At high P the new lines appear at the low energy side of the X line. They are labeled X_2^+ and X_2^- in the σ^+- and σ^- polarization, respectively, and correspond to the emission of two exciton states. The energy gap between these lines is equal to that between lines X^+ and X^-. This is in agreement with the transition scheme in Fig. 8 because the splitting of the X_2 line is completely determined by the splitting of the final exciton state.

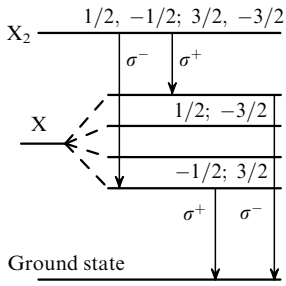

Figure 8. Scheme of the optical transitions for QD excitons and biexcitons with and without magnetic field.

As follows from Fig. 8 Δ_{XX} should be defined as the energy gap between the lines X_2^- and X^+ whereas the gap between the exciton and two exciton complex emission lines in the same polarization corresponds to the binding energy of two excitons with opposite spins of both the electrons and the holes, Δ_{XX}^0. Figure 9 shows that the magnetic field decreases Δ_{XX} strongly whereas the change of Δ_{XX}^0 is within experimental error. This means that the decrease of Δ_{XX} is mainly due to the Zeeman splitting of electron and hole states, whereas magnetic field induced rearrangement of electron and hole wave functions has a very small effect.

To conclude, the experimental studies of multiexciton complexes confined in QDs have shown that an exciton-exciton interaction in the two exciton complex enhances its confinement and that this effect increases with decreased dot size. The magnetic field normal to the QW plane has small influence on the binding energy of two excitons with opposite spins of two electrons and holes. The three exciton complex is confined only by the QD geometric confining potential. The magnetic field strongly reduces the exciton – exciton repulsion in such a complex when the magnetic length becomes smaller than $L_{x,y}$.

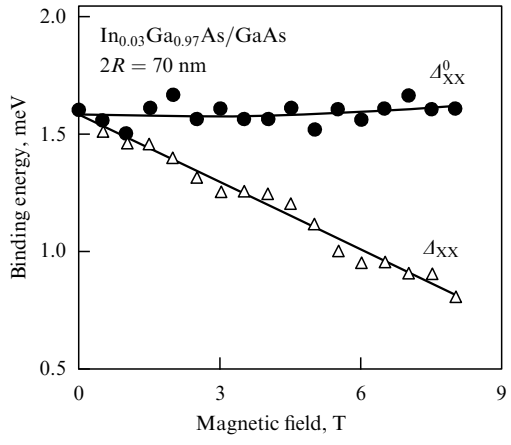

Figure 9. Magnetic field dependence of binding energy for two excitons with similar (Δ_{XX}) and opposite (Δ_{XX}^0) spins of both electrons and holes.

This work was supported in part by the Volkswagen Foundation and the Russian program "Solid State Nanostructure Physics" and "Fundamental Spectroscopy".

References

1. Schmitt-Rink S, Miller D A B, Chemla D S *Phys. Rev. B* **35** 8113 (1987)
2. Bryant G W *Phys. Rev. B* **41** 1243 (1990)
3. Hu Y Z et al. *Phys. Rev. Lett.* **64** 1805 (1990)
4. Brunner K et al. *Phys. Rev. Lett.* **73** 1138 (1994)
5. Steffen R et al. *Phys. Rev. B* **54** 1510 (1996)
6. Demel T et al. *Phys. Rev. Lett.* **64** 788 (1990)
7. Maksym P A, Chakraborty T *Phys. Rev. Lett.* **65** 108 (1990)
8. Andreev A A, Blanter Ya M, Lozovik Yu E *Int. J. Mod. Phys B* **9** 1843 (1995)
9. Halonen V, Chakraborty T, Pietilainen P *Phys. Rev. B* **45** 5980 (1992)
10. Bockelmann U *Phys. Rev. B* **50** 17271 (1994)
11. Bayer M et al. *Phys. Rev. Lett.* **74** 3439 (1995)
12. Rinaldi R et al. *Phys. Rev. Lett.* **77** 342 (1996)
13. Zrenner A et al. *Phys. Rev. Lett.* **72** 3382 (1994)
14. Steffen R et al. *Appl. Phys. Lett.* **68** 223 (1996)
15. Kulakovskiĭ V D, Pikus G S, Timofeev V B *Usp. Fiz. Nauk* **135** 237 (1981) [*Sov. Phys. Usp.* **24** 815 (1981)]

Anomalous transport and luminescence of indirect excitons in coupled quantum wells

L V Butov

The electron – hole (e – h) interaction in a neutral e – h system can result in the condensation of bound e – h pairs (excitons) [1]. In case of a dilute exciton gas ($na_B^d \ll 1$, where a_B is the exciton Bohr radius, n is the e – h density, and d is the dimensionality) the excitons can be considered as point Bose particles and the condensation is analogous to the Bose – Einstein condensation of bosons, while for a dense e – h system ($na_B^d \gg 1$) the condensed state is analogous to the BCS superconductor state.

The condensation conditions can be achieved only if the temperature of the excitons is below a critical temperature, T_c. This criterion is hard to achieve experimentally. Due to e – h recombination the excitons in semiconductors have a finite lifetime which results in an increase of the exciton temperature. Therefore, to search for exciton condensation, semiconductors with a long exciton lifetime are selected. Degenerate Bose – Einstein statistics have been observed for excitons in Cu_2O [2] and in Ge [3]. Recently the passing of the exciton condensate phase boundary for excitons in Cu_2O was reported [4].

The semiconductor quantum well (QW) structures provide an opportunity for the experimental realization of a quasi-two-dimensional exciton condensate. It has been

predicted that the critical conditions for the exciton condensation in QWs can be drastically improved by a high magnetic field perpendicular to the well plane [5, 6]. At zero magnetic field in a dense e–h system T_c is determined by the dissociation of condensed pairs; on the contrary, the dissociation is negligible in the dilute limit, only the exciton center of mass excitations are relevant: T_c is reached when the $k = 0$ state is empty. In the high magnetic fields the internal structure of the exciton and the motion of its center of mass are coupled [6]: the emptying of $k = 0$ states is accompanied by the exciton's dissociation. This coupling results in a strong modification of the density dependence of T_c. In the high field limit the critical temperature for the exciton condensation was calculated to be

$$T_B = \frac{E(1-2\nu)}{2\ln(\nu^{-1}-1)},$$

where E is the magnetoexciton binding energy and $\nu = n/n_{LL}$ is the Landau level filling factor [5, 6]. At low densities T_B is much higher than the zero field critical temperature which has a roughly linear density dependence

$$T_0 \propto \frac{2\pi\hbar^2 n}{m\ln(nS)},$$

where m is the exciton mass and S is the system area [7].

The precursor of exciton condensation in QWs at high magnetic fields, namely the formation of excitons in a dense e–h system has been observed in InGaAs/GaAs QWs [8]. However, due to the relatively short exciton lifetime in single QWs, and hence the high exciton temperature, the condensation phase boundary was not passed. The e–h recombination rate is strongly reduced in coupled QWs (CQWs) where electrons and holes are confined in different QWs. Due to the long recombination lifetime of indirect (interwell) excitons CQWs are considered a good candidate for the observation of exciton condensation [5, 9–11].

What are the expected specific properties of the exciton condensate which could be measured by experiment? The condensation of interacting excitons should be accompanied by the appearance of exciton superfluidity [5, 6, 9, 10]. Besides this, the condensation should be accompanied by a change of the excitons' optical properties. In particular, exciton condensate superradiance is expected to appear which can be detected as a strong increase of the exciton oscillator strength, and, correspondingly, a reduction of the exciton radiative lifetime [12]. The latter effect has the following origin: the exciton oscillator strength increases with increasing coherent area of the exciton [13]; for the condensed excitons the whole size of the condensate is a coherent area which implies a large exciton oscillator strength.

An unavoidable property of QWs is the existence of a random potential (determined mainly by the interface fluctuations for narrow QWs). The PL line shape is mainly determined by the random potential, therefore, it can hardly be used for the analysis of the exciton condensation in QWs [14]. The random potential strongly influences the properties of the exciton condensate in QWs. For zero potential fluctuations the exciton condensate is homogeneous in space and spreads over the sample (for the net repulsive interaction between excitons which is the case for indirect excitons in CQWs [11, 15]). For nonzero potential fluctuations a random array of normal areas and condensed domains is formed. With an increase of the potential fluctuations the sizes of the condensed domains are reduced and at large potentials the exciton condensate disappears. Therefore, in order to observe the exciton condensate, good samples with small potential fluctuations are needed.

We performed an experimental study of the transport and luminescence of indirect excitons in AlAs/GaAs CQWs at high magnetic fields and low temperatures. The possibility of exciton condensation in these CQWs is analyzed by comparison of the experimental data with the expected properties of exciton condensate.

Electric field tunable n^+-i-n^+ AlAs/GaAs CQW structures were grown by MBE. The i-region consists of a 40 A AlAs and 30 A GaAs layer, surrounded by $Al_{0.48}Ga_{0.52}As$ barrier layers (Fig. 1). In the direct regime (external gate voltage $V_g \gtrsim 0.5$ V) both electrons and holes are confined in the GaAs QW. In the indirect regime ($V_g \lesssim 0.5$ V) electrons are in the AlAs QW and holes in the GaAs QW. The electron state in AlAs is constructed from the X_z minima of the conduction band which is the main origin of the long lifetime of the indirect exciton. At $V_g \leqslant 0$ the lifetime is sufficiently long to allow for a thermalization of indirect excitons down to temperatures about 1 K. At the same time, the effective spatial e–h separation is small, about 40 A. The small e–h separation is important as the calculated critical temperature for exciton condensation in high magnetic fields is proportional to the magnetoexciton binding energy (see above). Carriers were photoexcited in the GaAs QW either by a cw dye laser ($\hbar\omega = 1.85$ eV) or a pulsed semiconductor laser ($\hbar\omega = 1.8$ eV, pulse duration 50 ns).

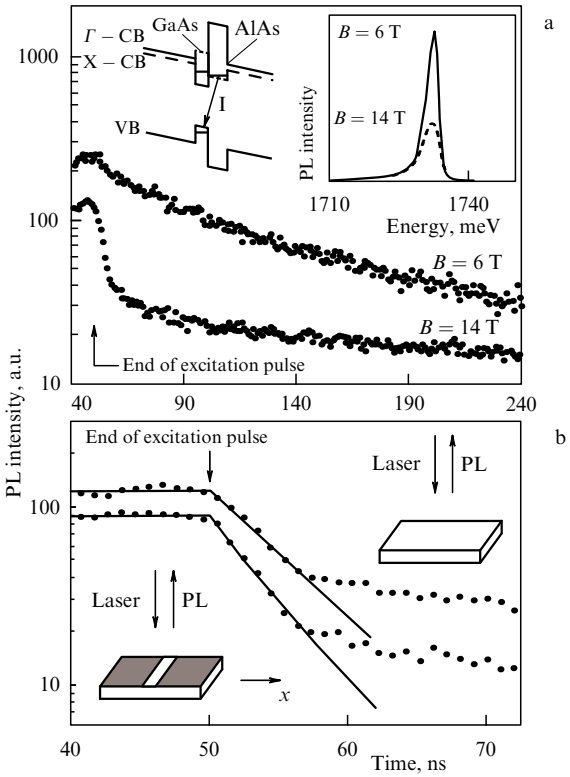

Figure 1. PL decay curves for the unmasked part of the sample at $V_g = 0$, $T = 350$ mK, and $B = 6$ and 14 T(a). Right insert: corresponding time integrated PL spectra. Left insert: band diagram of an AlAs/GaAs CQW in the indirect regime. The PL decay curves for the unmasked (upper curve) and the masked (lower curve) part of the sample for $B = 14$ T, $T = 350$ mK and $V_g = 0$ (b). The thin lines are the fitting curves for the initial times of the PL decay.

We first analyze the exciton transport. The PL decay curves at $T = 350$ mK and $B = 6$ and 14 T are shown in Fig. 1a. There is a clear difference in the initial PL intensity decay. The initial decay time τ is plotted against the magnetic field in Fig. 3c. At $B \lesssim 7$ T the decay is slightly non-exponential with a relatively long time constant. At higher magnetic fields a fast initial decay is followed by a slow decay at greater times. In the indirect regime the integrated PL intensity is much smaller than in the direct regime. Therefore, in the indirect regime the radiative lifetime, τ_r, is much larger than the non-radiative lifetime, τ_{nr}, and $\tau \approx \tau_{nr}$. It was found that in the narrow CQW structures τ_{nr} is mainly determined by the exciton transport to non-radiative recombination centers (NC) [16]. Therefore, the variations of τ in our CQWs may reflect the changes in the exciton transport. Under this assumption, the observed magnetic field dependence of τ implies that the increase of B first leads to a small reduction of the exciton diffusivity and then to a strong increase (Fig. 3c).

For direct measurements of exciton transport we used a time-of-flight technique: the PL decay from an unmasked part of the sample was compared with the PL decay from a part of the sample which was covered by a non-transparent mask, leaving an array of 4 μm wide stripes uncovered separated from each other by 32 μm. Excitation and detection of the PL signal were performed by means of an optical fiber with a diameter of 100 μm positioned either in front of the masked or unmasked part of the sample. Figure 1b shows an example of the PL decay curves for the unmasked and the masked part of the sample. For the PL decay in the masked part of the sample, due to the diffusion of excitons underneath the metal covered regions, the variation of the exciton density is described by

$$\frac{\partial n}{\partial t} = D\,\frac{\partial^2 n}{\partial x^2} - \frac{n}{\tau}\,,$$

where D is the exciton diffusion constant describing the exciton transport at the initial times of the PL decay. For the PL decay in the unmasked part of the sample the term $D\,\partial^2 n/\partial x^2$ can be neglected due to the large size of the excitation spot. The difference in the PL decays for the unmasked and the masked part of the sample can be presented by the time evolution of the ratio between the PL intensities,

$$R(t) = \frac{I_{PL}^{unmasked}(t)}{I_{PL}^{masked}(t)}\,.$$

Typical examples are shown in Fig. 2. The constant value of $R(t)$ during the PL decay implies that the exciton diffusion underneath the metal covered regions in the masked part of the sample is absent. The higher D, the stronger $R(t)$ deviates from being constant. Figure 2 shows that the deviation of $R(t)$ from constant is strongest at the beginning of the PL decay, and reduces with time during the decay (for any T and B). The thin lines in Fig. 2 are the fitting curves for the initial times of the PL decay which use D as a fitting parameter (τ is determined separately from the PL decay for the unmasked sample).

The magnetic field dependence of D at $T = 350$ mK is shown in Fig. 3e. D at first slightly decreases with B (this decrease is within the error bars) and then strongly increases. The temperature dependence of τ and D for $B = 6$ T and 14 T

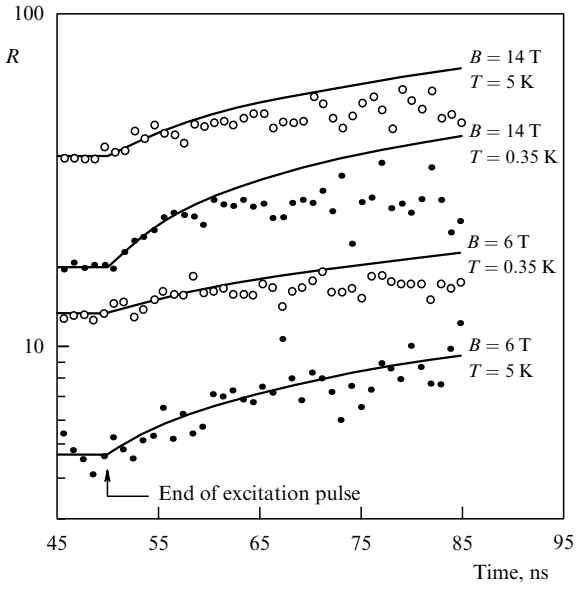

Figure 2. Time dependence of the ratio between PL intensities from the unmasked and the masked part of the sample at $V_g = 0$. The curves are shifted in vertical axis for clarity. Thin lines are the fitting curves for the initial times of the PL decay.

is shown in Figs 3d and 3f. The data for $B = 6$ T represent typical variations of τ and D at low magnetic fields while the data for $B = 14$ T are characteristic for high fields where rapid exciton transport is observed at low temperatures. Figure 3 shows that at $B = 6$ T an increase of T results in an increase of D and a reduction of τ. Contrary to this, at $B = 14$ T an increase of T results in a reduction of D and an increase of τ at $T \lesssim 5$ K. Only at higher temperatures τ starts to drop approaching the behavior observed for low magnetic fields. In all experiments an increase (reduction) of τ corresponds to a reduction (increase) of D. This confirms the assumption that τ is determined by the exciton transport to non-radiative recombination centers. The differential decay time increases with the delay time (Fig. 1a) which is consistent with the reduction of the exciton diffusion coefficient with the delay time (Fig. 2).

At low magnetic fields ($B \lesssim 7$ T), the temperature and magnetic field dependences of τ and D (Fig. 3c – f) are typical for thermally activated exciton transport in a random potential: at $B = 0$ an analogous reduction of the PL decay time and increase of the exciton diffusivity with increasing T has been observed in AlAs/GaAs type-II superlattices [16]; the monotonic reduction of the exciton diffusivity with increasing magnetic field can be qualitatively explained by the increase of the magnetoexciton mass and is in a qualitative agreement with the theoretical consideration of single exciton transport in AlAs/GaAs CQWs [17].

The increase of D which is observed at high magnetic fields and low temperatures (Fig. 3c, e) can not be explained in terms of single exciton transport. A possible explanation for this effect is the onset of exciton superfluidity. With increasing temperature the rapid exciton transport disappears, and at $T \gtrsim 5$ K the usual increase of the exciton diffusivity with temperature is recovered (Fig. 3d). As was discussed above, for exciton condensation in the presence of a random potential, superfluid domains with boundaries determined by the in-plane potential profile are expected to form.

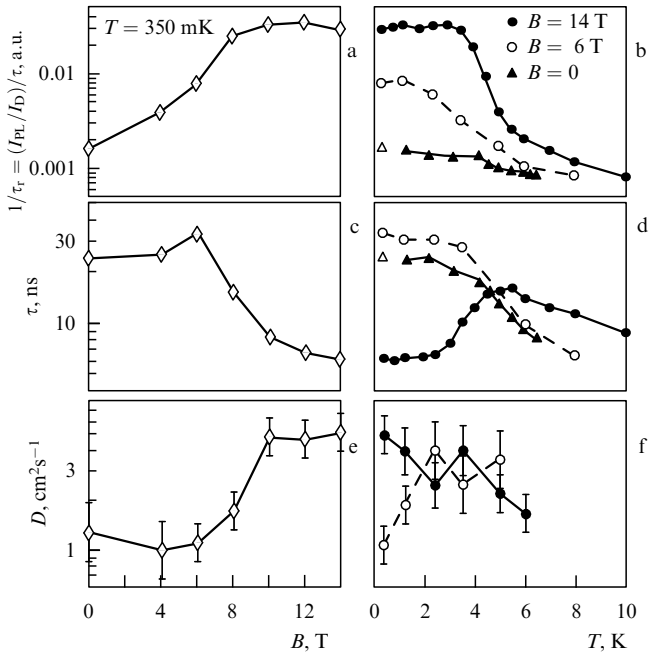

Figure 3. Magnetic field dependence of the inverse radiative lifetime of indirect excitons $\tau_r^{-1} = (I_{PL}/I_D)\tau^{-1}$ (a), the initial decay time τ (c), and the exciton diffusion coefficient D (e) at $T = 350$ mK and $V_g = 0$. Temperature dependence of $\tau_r^{-1} = (I_{PL}/I_D)\tau^{-1}$ (b), τ (d), and D (f) at $V_g = 0$, and $B = 0$, 6 and 14 T.

Therefore on a large scale the exciton transport is the transport in a disordered array of normal and superfluid regions which are determined by potential fluctuations. In the normal parts of this array the exciton diffusion coefficient increases with T and decreased with B, while in superfluid regions the opposite occurs — decreasing with T and increased with B. The measured exciton transport characteristics are averaged over the normal and superfluid regions in the excitation spot; the relatively low value of D, characteristic for the observed rapid exciton transport, can be understood in such a picture.

The superfluidity should disappear with the reduction of the exciton density at the critical density which is temperature dependent. Due to the low level of the PL signal from the masked part of the sample we used only the maximum excitation power of the laser which corresponded to an average initial exciton density of $\sim 10^{10}$ cm^{-2}; we were not able to measure the excitation density dependence by the time-of-flight technique. Indirectly, the exciton density dependence is revealed in the time evolution of the PL decay. At low T and high B the fast initial decay corresponding to rapid exciton transport is observed until the exciton density drops by several times (see Fig. 1); the subsequent decay is slow and corresponds to slow exciton transport (see Figs 1 and 2). The transition from the rapid initial to the slow subsequent exciton transport is sharp and corresponds to the expected disappearance of exciton superfluidity. We also investigated the excitation density dependence of the PL decay for the unmasked sample. These measurements show that at high B and low T the initial decay time increases with the reduction of exciton density which implies that the rapid exciton transport observed at high B and low T disappears with the reduction of exciton density.

Besides exciton superfluidity, another signature of the exciton condensation is an increase of the exciton oscillator strength (see above). The exciton oscillator strength is inversely proportional to the radiative exciton lifetime, τ_r, which can be directly derived from the measured τ and the time-integrated exciton PL intensity, I_{PL}. In the case of monoexponential PL decay, $\tau_r^{-1} = (I_{PL}/g)\tau^{-1}$, where g is the generation rate. This formula is already enough to show the variations of τ_r, but does not gives its absolute value as g is unknown. For an estimate of g the quantum efficiency of the PL in the direct regime can be taken as unity. Then $g = I_D$ and $\tau_r^{-1} = (I_{PL}/I_D)\tau^{-1}$, where I_D is the measured integrated PL intensity in the direct regime. The magnetic field and temperature dependences of τ_r^{-1} are shown in Fig. 3a, b. It was found that the non-exponentiality of the PL decay introduces only unimportant corrections to the dependences. At $T = 350$ mK, τ_r^{-1} strongly increases with B (Fig. 3a). At high fields, τ_r^{-1} strongly falls with T, while at $B = 0$ it only weakly depends on T (Fig. 3b). The anomalously large τ_r^{-1} observed at high B and low T is consistent with the large exciton oscillator strength expected for the exciton condensate. As in the case of the transport measurements, in our experiments the average value of τ_r^{-1} is measured, integrated over the sample area. With the reduction of the excitation power and hence the exciton density, τ_r^{-1} strongly decreases, which is consistent with the disappearance of the exciton condensate.

A spectacular effect was observed under cw photoexcitation in high magnetic fields, namely, a huge broad band noise in the integrated PL intensity of indirect excitons [18] (Fig. 4). The average variation of the integrated PL intensity under cw photoexcitation was similar to that under pulsed photoexcitation — first an increase and then a decrease of I_{PL} was observed. It is connected with the variations of τ_r and τ_{nr}. The noise is observed at low temperatures (insert in Fig. 4). The spectral position of the PL line is practically constant during the intensity fluctuations (insert in Fig. 4) which shows

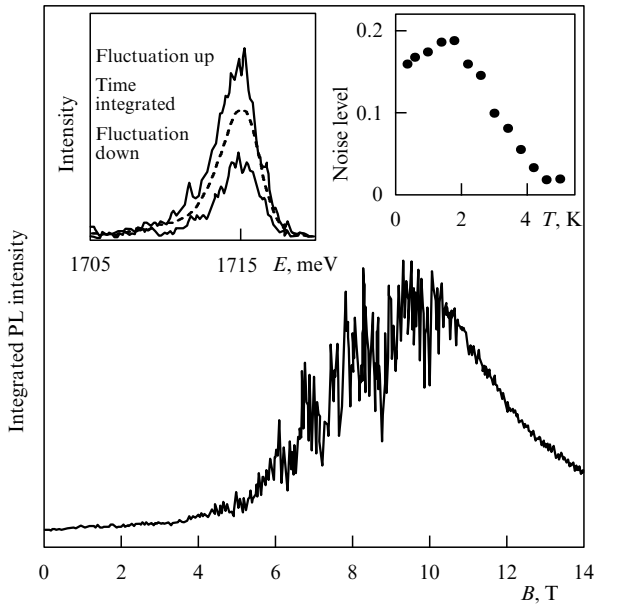

Figure 4. Magnetic field dependence of the integrated PL intensity of indirect excitons under cw photoexcitation at $T = 350$ mK and $V_g = -0.5$ V. Left insert: long time-integrated PL spectrum and PL spectrum integrated over 0.3 s in the noise regime at $B = 9$ T. Right insert: temperature dependence of the noise level $\langle \delta I_{PL} \rangle / \langle I_{PL} \rangle$ at $B = 9$ T.

that the noise cannot be related to the fluctuations of the CQW potential profile in the growth direction.

The appearance of the huge noise is strong evidence for the presence of coherence in the exciton system. Noise amplitude is known to be inversely proportional to the number of statistically independent entities in a system. Large noise amplitudes therefore denote that only a small number of entities exist in macroscopically large photoexcited region. The appearance of these macroscopic entities in the exciton system is consistent with the exciton condensation model. A condensed domain can be considered as one macroscopic entity. Due to the high oscillator strength of the exciton condensate, the PL signal of condensed excitons is much higher than for uncondensed ones. The formation and disappearance of condensed domains therefore results in fluctuations of the total PL signal. The noise appears in the range of B where τ_r^{-1} starts to increase and disappears in the range of B where τ_r^{-1} saturates and rapid exciton transport is observed. In the frame of the exciton condensation model the noise can be understood as the fluctuations near the phase transition connected with the instability of the condensed domains.

In conclusion, the observed set of anomalies in the transport and PL of indirect excitons in AlAs/GaAs CQWs is evidence for exciton condensation at low temperatures and high magnetic fields. The role of the magnetic field is the improvement of the critical conditions for the exciton condensation. The range of the magnetic fields studied can be divided into three parts. At low magnetic fields both the exciton transport and oscillator strength are characteristic for normal non-condensed excitons in a random potential: the diffusion coefficient increases with temperature, the oscillator strength only weakly depends on the temperature. At the highest studied magnetic fields both the exciton diffusion coefficient and the oscillator strength are anomalously large and decrease with temperature; this is consistent with the expected onset of exciton superfluidity and superradiance of exciton condensate. At intermediate magnetic fields a huge noise in the integrated PL intensity is observed under cw photoexcitation; the noise is consistent with fluctuations near the phase transition.

This work was performed in collaboration with A Zrenner, A I Filin, M Hagn, G Abstreiter, G Böhm, and G Weimann. We thank G E W Bauer, A B Dzyubenko, A Imamoglu, Yu M Kagan, V D Kulakovskiĭ, Yu E Lozovik, and B V Svistunov for interesting discussions. The work was supported financially by the Russian Foundation for Fundamental Research, the Russian Foundation for Nanostructures, and the Volkswagen Foundation.

References

1. Keldysh L V, Kopaev Yu E *Fiz. Tverd. Tela* (Leningrad) **6** 6219 (1965)
2. Hulin D, Mysyrowicz A, Benoit a la Guillaume C *Phys. Rev. Lett.* **45** 1970 (1980)
3. Timofeev V B, Kulakovskii V D, Kukushkin I V *Physica B* **117 – 118** 327 (1983)
4. Lin J L, Wolfe J P *Phys. Rev. Lett.* **71** 1222 (1993)
5. Kuramoto Y, Horie C *Solid State Commun.* **25** 713 (1978)
6. Lerner I V, Lozovik Yu E *Zh. Eksp. Teor. Fiz.* **80** 1488 (1981) [*Sov. Phys. JETP* **53** 763 (1981)]
7. Kagan Yu M, unpublished; for the infinite 2D systems the critical temperature for a phase transition to a superfluid state at $B = 0$ also roughly linearly depends on the density, see e.g. Fisher D S, Hohenberg P C *Phys. Rev. B* **37** 4936 (1988)
8. Butov L V et al. *Phys. Rev. B* **46** 12765 (1992)
9. Lozovik Yu E, Yudson V I *Zh. Eksp. Teor. Fiz.* **71** 738 (1976) [*Sov. Phys. JETP* **44** 389 (1976)]
10. Shevchenko S I *Fiz. Nizk. Temp.* **2** 251 (1976) [*Sov. J. Low Temp. Phys.* **2** 251 (1976)]
11. Zhu X et al. *Phys. Rev. Lett.* **74** 1633 (1995)
12. Bauer G E W, in *Optics of Excitons in Confined Systems* (Institute of Physics Conference Series No. 123, Eds A D'Andrea et al.) (Bristol, Eng.; Philadelphia: Institute of Physics, 1992) p. 283
13. Rashba E I, Gurgenishvilli G E *Fiz. Tverd. Tela* (Leningrad) **4** 1029 (1962) [*Sov. Phys. Solid State*]
14. Kash J A et al. *Phys. Rev. Lett.* **66** 2247 (1991)
15. Yoshioka D, MacDonald A H *J. Phys. Soc. Jpn.* **59** 4211 (1990)
16. Gilliland G D et al. *Phys. Rev. Lett.* **71** 3717 (1993)
17. Dzyubenko A B, Bauer G E W *Phys. Rev. B* **51** 14524 (1995)
18. Butov L V et al. *Phys. Rev. Lett.* **73** 304 (1994)

A self-assembled InAs quantum dot used as a quantum microscope looking into a two-dimensional electron gas

T Ihn, A Thornton, I E Itskevich, P H Beton, P Martin, P Moriarty, E Müller, A Nogaret, P C Main, L Eaves, M Henini

In the last decades our knowledge about two-dimensional electron gases (2DEGs) at low temperatures and in magnetic fields has tremendously grown and theoretical concepts have been developed describing their properties on a quantum mechanical basis and on a nanometer scale. Experiments are now desirable which test the predictions of these concepts not only on a macroscopic scale but using local probes of nm-size. We are able to probe the emitter 2DEG of a single-barrier tunneling device locally with a single InAs quantum dot [1 – 3]. The method has significant advantages over 2D – 2D tunneling experiments [4]. The dot is a local probe typically of 10 nm diameter and the tunneling characteristics are not smeared out by impurities. The discrete character of the dot state allows us to do energy spectroscopy by tuning the bias voltage. In contrast to conventional parallel magnetotransport measurements not only Fermi-level properties of the 2DEG can be observed but states (e.g. Landau levels) below the Fermi energy can be probed in a magnetic field [2, 3]. In addition, the properties of a single dot are of their own interest. Our measurements give us the opportunity to observe spin-splitting of the ground state of a single quantum dot.

The samples are single barrier n – i – n tunneling devices grown by MBE at 520 °C on the (100) surface of a GaAs n^+-substrate. Using the Stranski – Krastanov growth mode, self-assembled InAs quantum dots have been incorporated on the centre plane of the 10 nm AlAs barrier. The barrier is sandwiched between 100 nm undoped GaAs buffers on both sides. Graded n-type doping allows Ohmic contacts to be made on the top and the substrate side. Mesa structures typically of 50 μm diameter were fabricated by standard photolithography.

A typical dot size of 10 nm and a dot density of 10^{11} cm^{-2} was deduced from Scanning Tunneling Microscopy (STM) and Scanning Electron Microscopy (SEM) on similarly grown wafers. From cross-sectional transmission electron microscopy (XTEM) we get a direct insight into the wafer grown for the transport measurements. The height of the dots